

Effect of grain size modulation on the magneto- and electronic-transport properties of $\text{La}_{0.7}\text{Ca}_{0.3}\text{MnO}_3$ nanoparticles: The role of spin-polarized tunneling at the enhanced grain surface

P. Dey and T. K. Nath*

Department of Physics and Meteorology, Indian Institute of Technology, Kharagpur, West Bengal 721302, India

(Received 7 June 2005; revised manuscript received 28 December 2005; published 14 June 2006)

We have investigated the effect of nanometric grain size on magneto- and electronic-transport properties of single-phase, nanocrystalline, granular $\text{La}_{0.7}\text{Ca}_{0.3}\text{MnO}_3$ samples having an average grain size in the nanometric regime (14–27 nm). Based upon a spin-polarized tunneling mechanism, we have proposed a phenomenological model to explain the observed electronic transport behavior over the whole temperature range (20–300 K), especially the gradual drop of metal-insulator transition temperature with a decrease in grain size, while ferromagnetic-paramagnetic transition temperature remains almost constant. We have attributed the steeper low-temperature (~ 40 K) resistivity upturn in the smaller grain size sample rather than that of the larger grain size sample below their respective resistivity minima at T_{\min} to the increased value of charging energy, which has been estimated to be 13 K for a 17 nm sample and 0.026 K for a 27 nm sample. Most interestingly, magnetotransport measurements show that the magnitude of low-field magnetoresistance, as well as of high-field magnetoresistance remains constant up to sufficiently high temperature (~ 220 K) and then drops sharply with temperature. The effect gets more pronounced with the decrease in particle size. In order to explore the basic physics behind this unusual temperature dependence of magnetoresistance (MR), we have analyzed our data in light of a phenomenological model [P. Raychaudhuri *et al.*, Phys. Rev. B **59**, 13919 (1999)], based on the spin-polarized transport of conduction electrons at the grain boundaries. Analyzing our data following the theoretical perspective as proposed by S. Lee *et al.* [Phys. Rev. Lett. **82**, 4508 (1999)], we found that this strange temperature dependence of MR is decided predominantly by the nature of the temperature response of surface magnetization of nanosize magnetic particles. With the application of a magnetic field, strong freezing of surface spins occur at the defect sites [having strong pinning strength (k) of spins] of disordered grains surface as a consequence of competitive interactions between the grain boundary pinning strength (k) and the magnetic field. Thermal energy ($k_B T$), up to a considerably high temperature, remains unable to flip them from their strained condition, resulting in such a temperature insensitive behavior of MR as well as of surface spin susceptibility.

DOI: [10.1103/PhysRevB.73.214425](https://doi.org/10.1103/PhysRevB.73.214425)

PACS number(s): 75.47.-m, 72.25.-b, 73.63.Bd

I. INTRODUCTION

Transitional-metal oxides (TMO) with the perovskite structure have a long history of research and have been known as materials with a variety of interesting properties, such as electrical transport, magnetic, dielectric, and optical properties. The first renewal of interest in the perovskite TMO took place when the high-temperature superconducting (high- T_C) cuprates with layered perovskite structures were discovered.¹ The second renewal² was brought in by the important recent activities on mainly perovskite *manganites* of the form $\text{Re}_x\text{Ae}_{1-x}\text{MnO}_3$ where, $\text{Re}=\text{La, Nd, Pr, etc.}$ trivalent rare-earth ions and $\text{Ae}=\text{Sr, Ca, etc.}$ divalent alkaline-earth ions. A huge amount of studies of the colossal magnetoresistance (CMR) in this class of materials have been carried out in case of single crystals,^{3,4} thin film,⁵⁻⁷ and ceramic CMR materials,^{8,9} for both the search of the correct model to explain their magnetic, electrical, and magnetotransport properties and the possible application of them as magnetic sensors. The simplest explanation of the CMR observed for the manganites around ferromagnetic-paramagnetic Curie temperature (T_C) is given in terms of the double-exchange (DE) model. However, the physics of the extraordinary magnitude of CMR (Ref. 2) is obviously more complex. There are other

important factors than in the above simplest DE scenario, e.g., electron-lattice interaction, antiferromagnetic superexchange interaction between the t_{2g} local spins, intersite exchange interaction between the e_g orbitals (orbital ordering tendency), intrasite and intersite Coulomb repulsion interactions among the e_g electrons, etc.¹⁰ In spite of a number of models proposed so far; the sensitive balance between those competing mechanisms, in such a diversified rich physical systems having correlated degrees of freedom of charge, lattice, spin, and orbital ordering has not been clearly understood.

Regarding technological aspects, in those cases, magnetic fields of several T are typically required to obtain such a large MR effect near T_C . Further, the large MR associated with T_C is restricted to a narrow temperature range, and the large resistivity near T_C would give rise to high levels of electrical noise. All these collectively make these materials unworthy for real field sensing device applications. Moreover, low-field MR (LFMR) (Refs. 11–15) in polycrystalline manganites, which seems to have potential for possible sensor applications, is very much pronounced at low temperature and drops sharply with increasing temperature. Manganites thus remain unable to refute the early criticisms about their wide technological relevance.

It is well known that finite-size effects play a central role in physics, from the appearance of discrete energy levels in quantum dots to governing regimes of fluid flow. Recently, structural transitions driven by size, such as shape transitions of coherent precipitates¹⁶ and magnetic phase transitions in ferroelectric nanosystems,¹⁷ have further highlighted the intriguing new physics that arises at reduced dimensionality. Currently, nanoscale magnetism provides a wealth of scientific knowledge and potentials for applications, which include magnetic recording media, ferrofluids, catalysis, magnetic refrigeration, medical diagnostic, bioprocessing, drug delivery system, miniaturized magnetic sensor applications, etc. When the size of the magnetic particles is reduced to a few nanometers, the magnetic particles exhibit a number of outstanding physical properties such as giant magnetoresistance, superparamagnetism, small coercivity, low Curie temperature, and low-saturation magnetization as compared to their bulk counterparts. It is generally believed that a high value of the surface-to-volume ratio with a large fraction of atoms residing at the grain boundaries is what differentiates them from the bulk materials in their properties. Several works in different nanometric systems indicate the surface effect as responsible for their apparent anomalous behavioral changes with reduced dimension. As for example, ac electrical transport measurements¹⁸ on nanocrystalline nickel oxide pellets show that different relaxation processes are active in the grain interior and the grain boundary and that the temperature dependences of these relaxation processes are markedly different. Such deviations^{19,20} in the electrical properties of nanostructured materials is thought to be due to the spatial confinement of free and bound charges and it could be further enhanced with an increase in the volume fraction of the highly disordered grain boundaries. Several transport property studies revealed that the volume fraction of grain boundaries plays an important role in determining the electrical properties of nanostructured materials. Similarly, magnetic properties²¹ of materials in the nanosize regime are found to be significantly different from those of the bulk. In the nanosize regime, the surface-to-volume ratio increases, so the net magnetic behavior is dominated by surface magnetic properties.^{22,23} For example, in the case of magnetic nanoparticles, the most controversial issue—the observed reduction of the saturation magnetization—has been afterwards interpreted in terms of random canting of the particles surface spins caused by competing antiferromagnetic exchange interactions at the surface as proposed by Coey.²⁴ In our recent work²⁵ we have shown how modified surface magnetization of nanosize polycrystalline $\text{La}_{0.7}\text{Sr}_{0.3}\text{MnO}_3$ (LSMO) grains can tune the temperature dependent property of LFMR, appearing from the spin-polarized tunneling mechanism.

A number of such investigations of the grain size (in the nanometric regime) effect on electrical, magnetic, and magnetotransport properties of perovskites $\text{La}_{1-x}\text{A}_x\text{MnO}_3$ have been recently published.^{13–15,26–35} Nevertheless, no definitive theory or understanding has yet been achieved regarding the nanosize effect on various physical properties of manganites. The proper physical explanation for large discrepancies between metal-insulator transition temperature T_P and ferromagnetic-paramagnetic transition temperature T_C and

the gradual drop of T_P with decrease in grain size while T_C remains almost constant, in the case of a nanomanganite system, still is a matter of debate. Moreover, to the best of our knowledge, among these reports, there have been no detailed investigations of the grain size effect on the temperature dependent behavior of LFMR, which is very much essential from the technological perspective. Again, in the case of nanodimensional system, several extrinsic effects dominate over that of intrinsic properties of the system, so it can be readily understood that the preparation procedure must have a profound influence on its physical properties.³¹ In fact, the preparation procedure determines the nature of the surface region of nanosize grains, which plays a very crucial role in electrical transport, magnetic, and magnetotransport behavior of nanodimensional systems.

In this paper, we reported on a detailed study of the effect of nanometric grain size on electrical and magnetotransport properties of a nanocrystalline $\text{La}_{0.7}\text{Ca}_{0.3}\text{MnO}_3$ (LCMO) sample, prepared through the chemical route “pyrophoric reaction process.” In this work our objective is twofold. First, we have carried out electrical transport studies on the series of LCMO samples, which reveal the fact that T_C [from complex ac susceptibility ($\chi = \chi' + i\chi''$) measurement] does not follow the shift of T_P towards lower temperature with decreasing grain size creating a vast zones of ferromagnetic-insulator (FM-I) behavior. This is a clear violation of the established phase diagram³⁶ with the particular stoichiometric composition and in agreement with previous work.^{13,34,35,37} Moreover, there is a resistivity upturn at very low-temperature regimes (~ 40 K), which is much steeper for the smaller grain size sample than for that of the larger grain size sample. No existing model proposed for clean manganite systems can describe these unusual electrical transport behaviors. Andrés *et al.*³⁷ proposed the concept of a conduction channel mechanism for polycrystalline manganites (grain size in the range of $1.5 \mu\text{m}$ to 12 nm), based upon the nature of connectivity between grains. But their model only takes care of the macroscopic grain boundary effect on the conduction mechanism without providing any information on the microscopic transport mechanism of conduction electrons. Later, Yuan *et al.*³⁸ discussed the transport phenomena for polycrystalline manganites in the light of spin-polarized tunneling (SPT) model³⁹ with a major consideration about the size of grain, which is essentially larger than 100 nm (i.e., micron size particle) for their case. But the paper³⁸ does not clearly provide any physical explanation for gradual drop of T_P with decreasing grain size and the low-temperature resistivity minima observed in the nanomanganite system. In order to address this problem, here we propose a phenomenological model based upon the SPT mechanism to give a plausible physical explanation of the observed electrical transport behavior over the whole temperature range studied (20 – 300 K). Enough effort has been made to understand clearly the different issues, specifically (a) gradual drop of T_P with decrease in grain size, while T_C remains almost constant, and (b) steeper low-temperature resistivity upturn with the decrease in grain size. Moreover, we found that charging energy (E_C), which has been ignored in previous work,³⁸ plays a vital role in case of nanodimensional

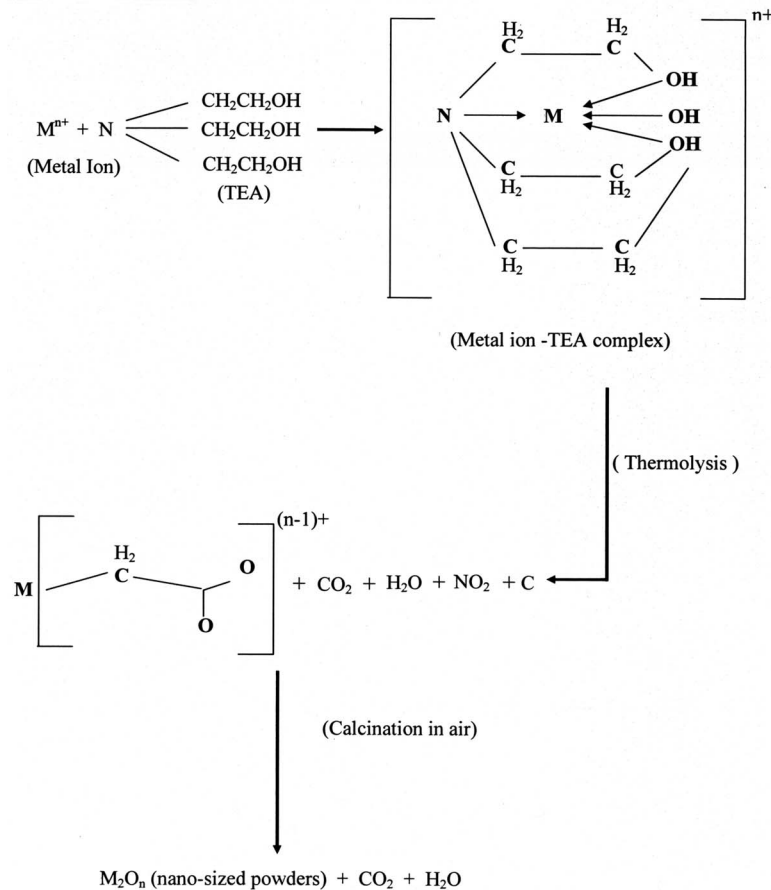
manganites. Recent work also supports this conception about the important key role of E_C^{40} in the case of nanosize manganites.

Secondly, we have performed a detailed study of the effect of nanometric grain size on magnetoresistance (MR), especially its temperature and magnetic field dependence. Very interestingly, MR measurements of these samples at both low (LFMR) as well as high fields (HFMR) show that the magnitude of MR remains almost constant up to sufficiently high temperatures (~ 220 K) and then drops substantially with temperature. This is no doubt a noticeable departure from the usually reported¹¹⁻¹⁵ behavior of a sharp drop of MR with increasing temperature. This temperature insensitive flat plateau region of MR increases with the decrease in grain size. In order to explore the basic physics behind this temperature dependence of MR, we have analyzed our data using a phenomenological model¹² based on the SPT of conduction electrons at the grain boundaries. Analyzing our data following the theoretical perspective as proposed by Lee *et al.*,⁴¹ we have attributed this exotic temperature dependence of MR to the nature of the temperature response of surface magnetization (M_S) of the nanosize grain, the role of which becomes very much dominant for our nanodimensional manganite system.

II. EXPERIMENTAL DETAILS

Nanometric particles of $\text{La}_{0.67}\text{Ca}_{0.33}\text{MnO}_3$ (LCMO) were prepared from high-purity La_2O_3 , $\text{Mn}(\text{CH}_3\text{COO})_2$, CaCO_3 by a pyrophoric reaction process. We have employed an aqueous solution of the requisite amount of compounds in stoichiometric proportions. Then triethanolamine (TEA) is added with these solutions in such a way that the metal ions to TEA ratios in the starting solutions are maintained at 1:1:4 (La, Ca: Mn: TEA=1:1:4), to make a viscous solution. The clear solutions of TEA complexed metal nitrates are evaporated on a hot plate at 180°C with constant stirring. The continuous heating of these solutions causes foaming and puffing. During evaporation, the nitrate ions provide an *in situ* oxidizing environment for TEA, which partially converts the hydroxyl groups of TEA to carboxylic acids. When complete dehydration occurs, the nitrate themselves are decomposed with the evolution of brown fumes of NO_2 leaving behind a voluminous, carbonaceous, organic based, black, fluffy powders, i.e., precursor powders with the desired metal ions embedded in its matrix. The chemical reactions involved in this method are as follows:

Chemical Reactions:



where M =metal ions. The dried carbonaceous mass is then ground to a fine powder and is calcined at various temperatures to get a series of LCMO nanocrystalline powders. The heat treatments of the precursor materials (in air 5 h) have been facilitated from 600–800 °C in steps of 50 °C.

Structural characterization of the nanocrystalline LCMO powders was carried out using x-ray powder diffraction (XRD) (models PW 1710 and PW 1810, Phillips) with monochromatic Cu-K_α radiation ($\lambda \sim 1.542 \text{ \AA}$) and by transmission electron microscopy (TEM) employing a JEOL 2010F UHR version electron microscope at an accelerating voltage of 200 kV. The dc resistivity was measured using four-probe method by Keithley 2000 digital Multimeter (6 and $\frac{1}{2}$ digit) in auto mode. A calibrated Pt-100 temperature sensor attached with a temperature controller (Scientific Instruments Series 5500) was used for the temperature measurement of the sample. Measurements were carried out in a temperature range of 80–300 K using a liquid nitrogen variable temperature cryostat. The dc resistivity measurements of some of the samples are carried out down to 20 K employing a closed cycle helium refrigerator cryostat along with a Keithley 181 Nanovoltmeter in auto mode and a calibrated Si-diode (DT-470) temperature sensor attached with a temperature controller (Scientific Instruments Series 5500). The entire setup was computer controlled through GPIB interface and the data acquisition was made by a PC (Pentium 4). MR measurements were carried out with the standard Van der Pauw technique at a constant 10 mA sample current in the temperature range of 80–300 K, in the transverse geometry (magnetic field perpendicular to the current, $J \perp H$) of magnetic field up to 10 kOe. The temperature measurement and control was made in a combination of a temperature controller (Lakeshore model 331S) and a calibrated Pt-100 sensor. The data accuracy during both resistivity and MR measurements was better than one part in 10 000.

III. RESULTS AND DISCUSSIONS

A. Structural characterization of the samples

In order to prove the nanodimension of each individual constituent particle of our powder LCMO samples, the structural characterization was made through x-ray powder diffraction (XRD) and by transmission electron microscopy (TEM). The as-prepared precursor powders were x-ray amorphous. Heat treatment of the precursors at 600 °C for 5 h resulted in single-phase LCMO powders. Figure 1 shows the XRD pattern of single-phase LCMO nanocrystalline powder calcined at 800 °C and the peaks were indexed on the basis of orthorhombic cell with $Pbnm$ space group symmetry. However, the XRD lines of these powders were very broad with large full width at half maximum (FWHM) (inset of Fig. 1), indicating the formation of nanocrystalline fine LCMO powders. The broad peaks observed in the XRD pattern of the nanocrystals arise from the finite number of diffracting planes within the finite size of the particle; the average grain size (D) in these cases is given by the Scherrer formula:⁴² $D = k\lambda / \beta_{\text{eff}} \cos \theta$, where k is particle shape factor (generally taken as 0.9), λ is the wavelength of Cu K_α radiation (1.542 Å), θ is the diffraction angle of the most intense

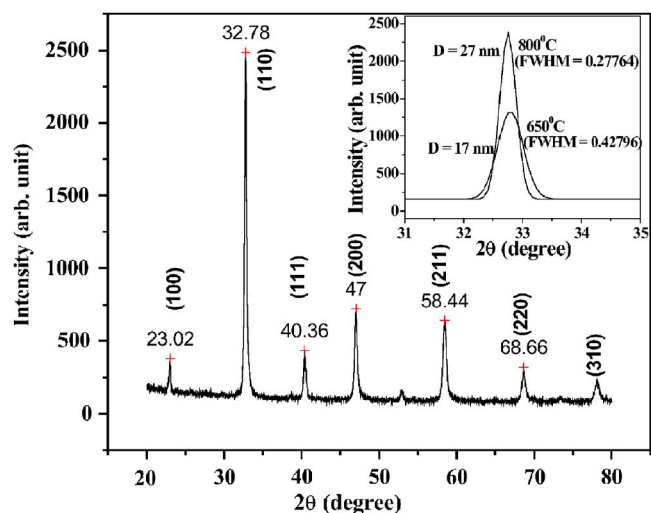


FIG. 1. (Color online) XRD pattern of the $\text{La}_{0.7}\text{Ca}_{0.3}\text{MnO}_3$ nanoparticles prepared at calcination temperature of 800 °C. Inset shows the variation of FWHM with calcination temperature.

peak (110), and β_{eff} is defined as $\beta_{\text{eff}}^2 = \beta_m^2 - \beta_s^2$, where β_m and β_s are the experimental FWHM of the present sample and the FWHM of a standard silicon sample, respectively. Increase in the calcinations temperature from 600 to 800 °C, resulting in the sharpening of the diffraction lines (inset of Fig. 1), with an increase in intensity. The values of thus obtained D are within 14–27 nm for LCMO grains calcined at different temperatures. The smallest average grain size (14 nm) of the LCMO sample achieved in the pyrophoric reaction process is small enough for the required rotation of the grains (overcoming its inertia) stimulated by the desired heat treatment-calcinations process, so as to align the crystallographic axes of two or more grains and consequently increase the size of the grains. However, this procedure of determining grain size is an indirect way to estimate the grain size.

Structural characterization through TEM is a rather direct way that provides visual demonstration to estimate grain size exactly. Figure 2 shows a typical TEM image of nanocrystals of LCMO calcined at 650 °C. TEM was done on the powders dispersed in a solvent and mounted on a carbon grid. Figure 2(a) shows bright field images of a nanocrystalline LCMO sample. The images show an abundance of nearly spherical particles whose size distribution is given by the histogram shown in Fig. 2(b), the histogram being obtained by analyzing several frames of similar bright field images. We find that the particles have an average size of 17 nm, which is in close agreement with the results obtained from XRD studies (~ 17 nm). Selected area diffraction pattern (SAED) [Fig. 2(c)] obtained from a single grain shows the single-crystalline nature of the LCMO nanograins. The high-resolution image (HRTEM) is shown in Fig. 2(d).

It was reported that in an ideal monodisperse system, single magnetic domain should be expected for manganite particles with a size lower than a critical value $D_C \sim 70$ nm.⁴³ Though our real system is polydisperse in nature, but the reasonably narrow distribution of particle sizes assures us that even for our largest grain sample (27 nm) the maximum

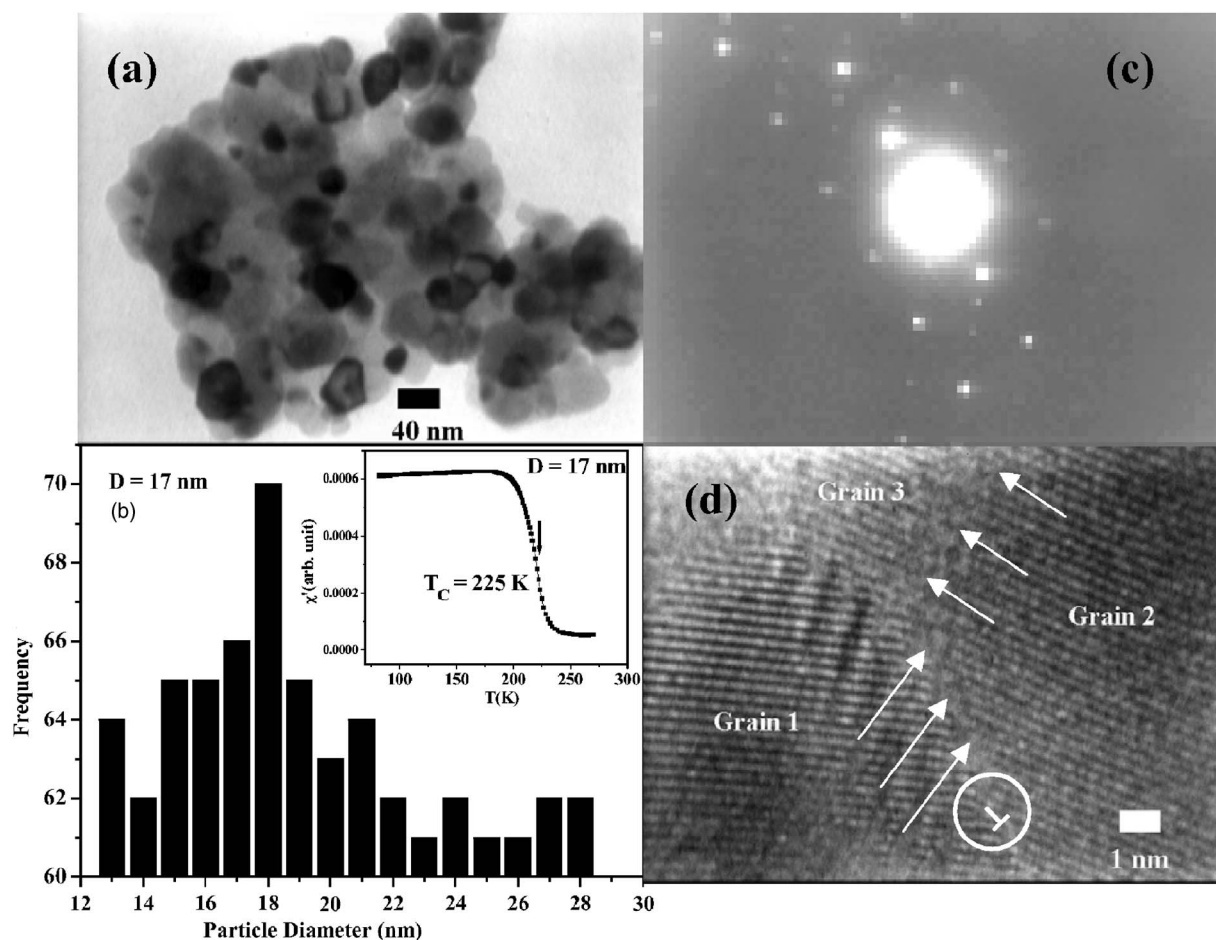


FIG. 2. (a) Transmission electron micrograph of LCMO sample calcined at 650°C . (b) Histogram showing the grain size distribution of our nanocrystalline LCMO sample calcined at 650°C . Inset shows the magnetic ac susceptibility of the LCMO sample having an average grain size of 17 nm, measured in the temperature range of 80–300 K. (c) Selected area diffraction (SAD) pattern of a single LCMO nanocrystal showing the single-crystalline nature of LCMO nanograins. (d) HRTEM image of the grain boundaries of three adjacent grains of LCMO nanocrystals. Image shows a high level of disorder (\uparrow marked) including dislocations (\perp marked) etc. at the faceted grain surface of the nanocrystals.

particle size is not expected to cross 70 nm. That is, finally we can assign the nature of the physical structure of this series of samples as an assembly of single magnetic-domain particles having grain size in the nanometric regime.

B. Electrical transport studies

For electrical resistivity measurements (ρ - T) down to a low-temperature (~ 20 K) range, powders were pressed and sintered at corresponding calcinations temperature for 30 min to weld the grains and to form a pellet. The effect of this sintering treatment is not expected to further increase the grain size since we have sintered the respective sample at its corresponding calcinations temperature. Therefore, the sintering effect can only be to glue one grain to the other. Figure 3 shows the normalized resistivity as a function of temperature for the series of LCMO nanocrystalline samples having different grain size. It is evident from Fig. 3 that with the decrease in average grain size, the metal-insulator transition temperature (T_p) shifts towards lower temperature. In comparison with single crystals or polycrystalline samples with

larger grain size ($\sim 20 \mu\text{m}$, prepared through solid state reaction technique) having $T_p \sim 262$ K, for our largest grain sample (27 nm) T_p appears at 195 K, while for our smallest grain sample (14 nm) it appears at 90 K, associated with a pronounced increase in resistivity over the whole temperature range studied. It is well known that electrical transport properties depend not only on the size of grains of the samples, but also on the porosity of the pellets. Therefore, in order to explore specifically the effect of nanometric grain size on the observed electrical conduction behavior (Fig. 3), first we should have a proper understanding about the effect of porosity of the pellets on the observed transport properties. In order to discriminate between the effect of porosity and grain size on the transport properties, our approach is to keep one parameter fixed and to see how the variation in other modifies transport properties. For this purpose we have carried out a series of calcination (T_{Cal}) and sintering (T_{S}) treatments on the samples with different combinations of temperatures and finally found one sample, calcined and sintered at 650°C and 1000°C respectively, having final grain size of the pellet 21 nm. This is a suitable sample to compare

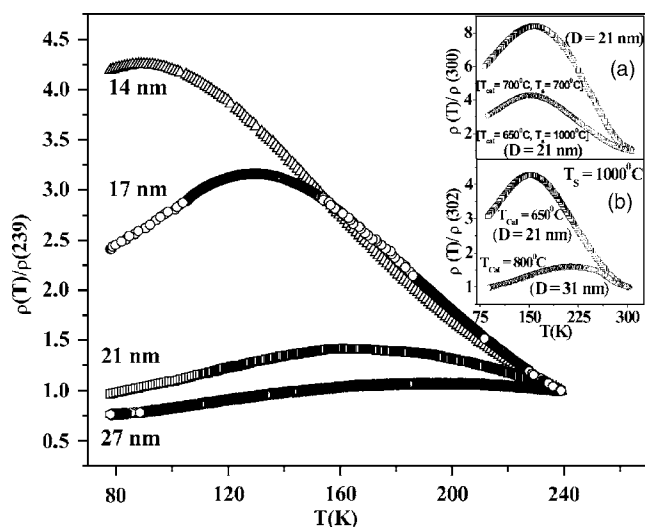


FIG. 3. Normalized reduced resistivity vs temperature for a series of nanocrystalline LCMO samples having average grain sizes of 14, 17, 21, and 27 nm in the temperature range of 80–300 K. Inset (a) shows the same plot for two samples having same average grain size (21 nm) but having a reasonably different porosity effect, whereas inset (b) shows the same for two samples having different grain sizes (21 and 31 nm) but having same porosity effect.

(ρ - T) behavior with that calcined and sintered at both 700 °C having a final average grain size of the pellet of 21 nm. Therefore, these two samples have the same grain size (21 nm), but the widely separated final sintering temperatures (700 °C and 1000 °C) implies that they should have reasonably different porosity effect. Inset (a) of Fig. 3 reveals that T_p for those two samples are almost same, which indirectly indicates the average grain size of the sample as the principal deciding factor of metal-insulator transition. On the other hand, in spite of identical average grain size of these two samples, it is found that there is an appreciable decrease in resistivity for the sample sintered at 1000 °C than that of sample sintered at 700 °C. The observed decrease in resistivity in this case can be attributed mainly to the reduced porosity with the increase in sintering temperature, as the average grain size of these two samples is the same (~ 21 nm). Thus from this result, it appears that porosity has an appreciable effect on the absolute value of resistivity, but it does not have any significant effect on metal-insulator transition phenomena. In order to substantiate this experimental finding, we have studied the reverse case also, where porosity effect is same but grain size is different between two samples. For this purpose, we have presented ρ - T curves [inset (b) of Fig. 3] for those two samples calcined at 650 °C and 800 °C and sintered at the same 1000 °C temperature, yielding the final grain size of the pellets as 21 nm and 31 nm, respectively. Porosity effect is expected to be excluded or same, for those two pellets sintered at such a high sintering (1000 °C) temperature. In this case also, with the decrease in average grain size from 31 to 21 nm and with the porosity effect expected to be same, T_p is clearly seen to be shifted at lower temperature along with a huge increase in resistivity. Here this increase in resistivity can be judiciously attributed entirely to the de-

TABLE I. Calcinations temperature (°C), grain size (nm), metal-insulator transition temperature (T_p), and ferromagnetic-paramagnetic transition temperature (T_c) of the series of nanocrystalline $\text{La}_{0.7}\text{Ca}_{0.3}\text{MnO}_3$ manganites.

Calcination T (°C)	Grain size (nm)	T_p (K)	T_c (K)
600	14	90	222
650	17	130	225
700	21	166	223
800	27	195	234

creasing grain size since porosity effect is same between those two samples. Thus it is obvious from this analysis that the absolute value of resistivity is influenced by both porosity and average grain size of the pellets almost to the same extent, whereas metal-insulator transition phenomena is influenced predominantly by average grain size of the samples with porosity of the pellets having very little influence on it. This means that in explaining the observed variation of T_p in the case of our series of samples [Fig. 3], we can as a whole attribute this mainly to the varying nanometric grain size and neglecting the porosity effect, whereas the observed increase in absolute value of resistivity [Fig. 3] we have to consider as due to the coupled effect of both increasing porosity (sintering temperature becomes smaller) and decreasing grain size.

Table I shows the T_p and T_c values of the series of LCMO samples that reveal the fact that T_c [inset of Fig. 2(b)] does not follow the shift of T_p with decreasing grain size, creating a vast zones of ferromagnetic-insulator (FM-I) behavior. One may assume the formation of small FM clusters, which are large enough to give a magnetic contribution but not to allow metallic conductivity. For single crystal, thin film, and polycrystals with a large grain size ($\sim \mu\text{m}$), $\text{La}_{0.7}\text{Ca}_{0.3}\text{MnO}_3$ samples electronic transition from insulator (I) to metal (M) is accompanied by a simultaneous paramagnetic (PM) to ferromagnetic (FM) transition at almost the same temperature, similar to the established phase diagram.³⁶ The origin of ferromagnetism and the close correlation between the magnetic and transport properties in $\text{La}_{0.7}\text{Ca}_{0.3}\text{MnO}_3$ are basically interpreted within the framework of the double-exchange model as proposed by Zener.⁴⁴ Thus in this FM-I regime with the particular stoichiometric composition, Zener double-exchange mechanism apparently appears to be violated. Existence of this FM-I region and the coupling of T_p with grain size, while T_c remains almost unaffected, demands close scrutiny of the conduction mechanism in the case of a nano-size granular manganite system. In a process of describing the conduction mechanism in the case of polycrystalline manganites, having a grain size down to 12 nm, Andrés *et al.*³⁷ proposed the concept of a conduction channel mechanism based upon the nature of connectivity between grains. But as the model only takes care of the macroscopic grain boundary effect on the conduction mechanism, it does not provide information on the microscopic transport mechanism of the conduction electrons. Hwang *et al.*¹¹ were the first to introduce SPT mechanism (proposed firstly by Helman and

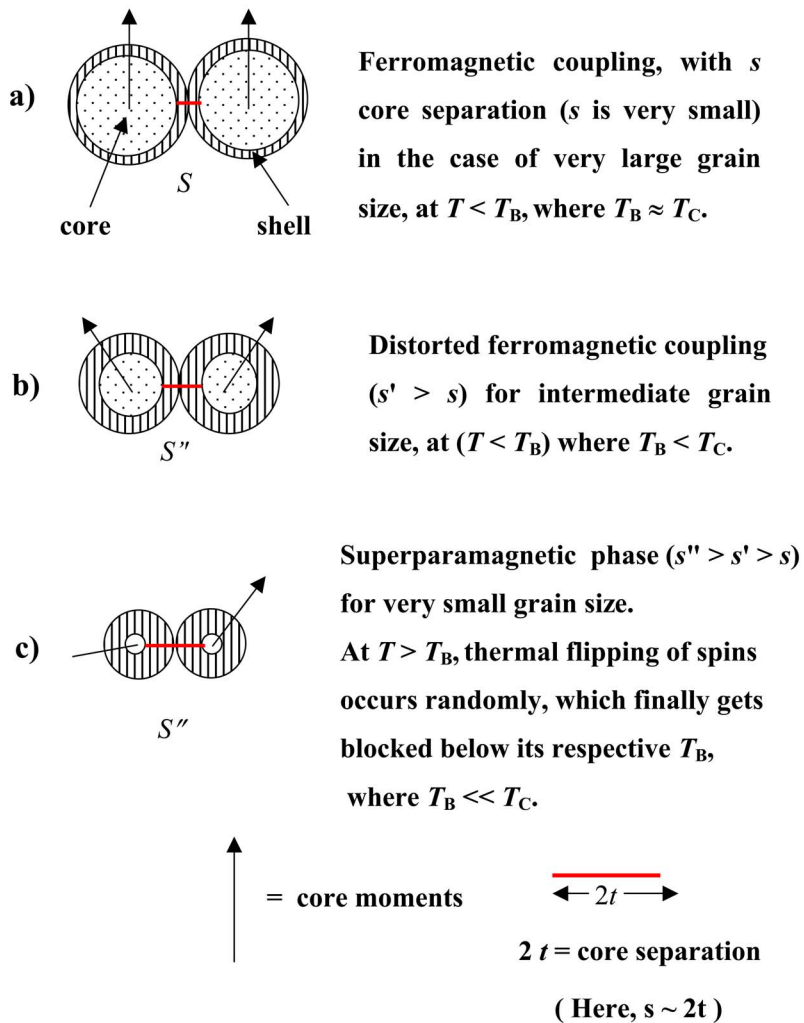


FIG. 4. (Color online) Phenomenological demonstrative representation of the possible ordering of core moments in the core-shell structure of nanometric manganite grains with the grain size as a variable parameter at different temperature ranges.

Abeles³⁹ in granular nickel films) in the case of manganites on the basis of a noteworthy feature of these materials, which is the high degree of spin polarization of the charge carriers, caused by the half metallic nature of these materials.⁴⁵ Later, Yuan *et al.*³⁸ discussed the transport phenomena for polycrystalline manganites in the light of the SPT model with a major consideration about the size of grain, which is essentially larger than 100 nm (i.e., micron size particle) for their case. However, to elucidate the underlying physics behind the existence of this FM-I region and especially the coupling of T_p with grain size, while T_C remains almost unaffected, in the case of our nanocrystalline LCMO sample (grain size is in the range of 14–27 nm), we have considered the microscopic transport mechanism of the conduction electrons, as suggested by the SPT model,³⁹ which will itself intrinsically take care of the macroscopic grain boundary effect on the conduction mechanism.³⁸

Now, before going into details of the conduction mechanism, especially into the explanation of metal-insulator transition, we would like to present a brief description of the physical structure of nanosize manganite grains based upon some previous reports. Practically, when the size of the manganite grain reduces to few tens of nanometers, we can assign a core-shell structure to them,^{15,28,46} where the inner part of the grain, i.e., the core, would have the same properties as

the bulk compound whereas the outer layer, i.e., shell (width t), would contain most of the oxygen defects and faults in the crystallographic structure, which would lead to a magnetically dead layer. It is a quite well-established fact that shell thickness (t) increases with the decrease in grain size.^{15,28,46} Basically, the net intercore barrier thickness ($s=2t+d$), namely the total shell thickness ($2t$) of two neighboring grains together with the intergranular distance (d) increases with the reduction of grain size. Our schematic diagram (Fig. 4) shows that with the decrease in grain size core separation ($s \sim 2t$) increases significantly with the thickness of the shell (t), even if we consider the grains to be in intimate contact ($d=0$) for all grain size samples. For polycrystalline CMR samples having an average grain size larger than 100 nm, d is reported³⁸ to be 1–2 nm (where $t \sim 0$). Zhang *et al.*¹⁵ reported t to be about 2 nm in magnitude for a manganite samples having a minimum grain size of 50 nm. That is, in that case, even if we consider two grains to be in intimate contact ($d=0$), s ($\sim 2t$) will be 4 nm. We are working in the range of 14–27 nm, thus in our case effective s is expected to be several nanometers; even for our largest grain (27 nm) sample, s is expected to be reasonably greater than 4 nm. Another important fact is that in absence of magnetic field the contributory portion of each individual grain to the magnetization is the core and not the shell, as in the absence of

applied magnetic field, net magnetization of the shell is considered to be zero (magnetically dead). Since, quite expectedly, the surface would contain most of the oxygen defects and faults in the crystallographic structure, that will lead to a magnetically disordered state. Again, at the manganite grain surface, there may be antiferromagnetic ordering⁴⁷ of the Mn spins due to the modification of charge state of the Mn ions. Thus, for simplicity, we consider a zero net magnetization ($M_S \approx 0$) to this shell in the absence of any magnetic field.

It can easily be understood that in the case of nanosize manganites, an appreciable amount of charging energy E_C (Ref. 48) ($\propto s/d$) is required for the generation of charge carriers. In our case, d is in the range of (~ 14 – 27 nm) and s is of the order of few nanometers, thus the ratio (s/d) has appreciable value. So, we cannot neglect E_C in the case of nanodimensional manganite grains, in contrast to the work by Yuan *et al.*³⁸ where this term was neglected in explaining the conduction mechanism for polycrystalline manganites having a grain size larger than 100 nm and where s is of the order of 1–2 nm. In this case, charge carriers are thermally activated, which means the generation of a large number of charge carriers, with appreciable energy E'_C ($E'_C > E_C$), takes place at a relatively high-temperature regime. But at a high-temperature regime, since there is considerable flipping of the magnetic moments of the grains as well as of spin of conduction electrons, the condition for SPT is not favorable. As a result, we observe an insulating behavior at a high-temperature ferromagnetic regime. But as the temperature decreases, spin-flipping will decrease; at a reasonably low-temperature range, they got blocked. Thermal energy is unable to flip them anymore. Now, at this low-temperature regime with the blocked state of spins, SPT of conduction electrons takes place, creating the so-called metallic regime. In order to elucidate the basic reason behind the drop of T_P with decreasing grain size, we have to correlate the above discussion with grain size. In this aim, first we would like to discuss the role of three major parameters, i.e., anisotropy energy, magnetic exchange energy, and thermal energy, determining the degree of ordering (or blocking) of the adjacent grain moments of the manganite samples in their ferromagnetic regime in the absence of a magnetic field, with the grain size as the variable parameter. Regarding anisotropy energy of each particle $E=KV$, where K is total anisotropy constant and V is the volume of each magnetic particle, we may say that since the volume of the core portion of the grain decreases appreciably with lowering grain size, the anisotropy energy of that portion of grains accordingly would get minimized. In fact, the core portion decreases even more sharply as shell thickness increases with decreasing grain size. Regarding exchange interaction, it results from the overlapping of the wave functions of the magnetic electrons in neighboring grains and it is expected that this exchange energy will decrease with an increase in intergrain separations. So following this we may assert that since decrease in grain size results in enhancement of core separation s (with the increase in t) between two neighboring grains (Fig. 4), magnetic exchange energy between adjacent grains (basically core) gradually decreases with the decrease in grain size. In fact, often magnetic particles are coated with non-

magnetic layers⁴⁹ to avoid exchange coupling among them through intimate contact in order to achieve noninteracting superparamagnetic particles. Accordingly, in the absence of a magnetic field, we can also suppose the core of our nanosize manganite grains as magnetic particles coated with a non-magnetic layer (shell), where the increasing shell thickness (t), as a result of decreasing grain size, causes the reduction of exchange coupling among grains (basically core). It means a considerably large s can even cause superparamagnetic phase having no exchange coupling among grains. Thus considering all practical conditions and extrinsic effects, we can qualitatively predict the mutual comparative behavior of anisotropy energy, magnetic exchange energy, and thermal energy, since within this frame we are not able to predict their exact comparative energy scale. It appears that with the decrease in grain size, exchange interaction between adjacent grains as well as anisotropy energy of the individual grain reduce significantly. As a direct consequence, the role of thermal energy, causing fluctuations of the core moments, gradually acquires increasing importance with the decreasing grain size and thermal energy can dominate over the magnetic exchange energy as well as anisotropy energy down to several temperatures below T_C . Thus with decreasing grain size, because of these increasing thermal fluctuations or dominating superparamagnetic effect, ordering of grains moments cannot be achieved down to several temperatures even far below T_C .

Figure 4 represents a general phenomenological demonstration of the possible ordering of core moments in the core-shell structure of nanometric manganite grains with the grain size as a variable parameter. It is obvious that in the temperature range, above paramagnetic-ferromagnetic transition temperature (T_C) of those respective samples (Table I), i.e., at $T > T_C$, there is no magnetic ordering in the system for any grain sizes. This situation is not depicted in Fig. 4 for any grain sizes. However, below T_C , where in this temperature range ($T < T_C$) intracore magnetic ordering takes place, i.e., each individual grain has a net magnetic moment for any grain size; the nature of intercore or intergrain magnetic ordering of core moments depends upon grain size. For comparatively larger size grains, as magnetic exchange energy and anisotropy energy are expected to be appreciable, as already discussed in the previous paragraph, intercore magnetic ordering, dominated by exchange and anisotropy energy, is expected to take place just below T_C where thermal energy is not supposed to dominate over those two energies or on magnetic ordering of the core moments in this case. This situation is depicted in Fig. 4(a), where core moments get blocked orderly because of the dominance of magnetic exchange energy and because of the ineffectiveness of thermal energy here blocking temperature of core moments $T_B \approx T_C$. For comparatively smaller size grains, where mainly exchange as well as anisotropy energy are very weak, as already discussed in the previous paragraph, thermal energy can dominate over those two; as a result, thermal flipping of core moments persists randomly even far below T_C and below a certain temperature when thermal energy is unable to flip the core moments, overcoming the anisotropy energy of each individual grains, i.e., at $T < T_B$ (T_B =blocking temperature), those core moments get blocked in a direction decided

by only the anisotropy axis of the individual grains. This situation is depicted in Fig. 4(c) where, unlike larger size grain [Fig. 4(a)], no proper ordering of adjacent core moments in the blocked state is possible in this case [Fig. 4(c)], since the final blocking of the core moments in this case of smaller size grains are decided only by the anisotropy axis of individual grains and more important point is that in this case $T_B \ll T_C$. Figure 4(b) is the intermediate case between these two, where T_B is supposed to be lower than T_C ($T_B < T_C$). Practically, this description of our model points to the fact that the blocking temperatures (T_B) of core moments are different for different grain sizes and the more subtle feature is that they (T_B) are lower for smaller grain sizes. Again, since our system is polydisperse in nature, there is a distribution in s ; therefore, one may expect a mixture of a superparamagnetic [Fig. 4(c)] and ferromagnetic or nearly ferromagnetic coupling [Figs. 4(a) and 4(b)] among the grains below T_C . Thus we may conclude from above discussion that for all samples with various grain sizes, three statuses, i.e., the ferromagnetic, distorted ferromagnetic, and superparamagnetic phases, are possible at various temperature ranges and the key is that for different grain sizes there are different blocking temperatures T_B , which are lower for smaller grain size.

Thus, finally the picture evolves that for comparatively smaller (average) grain size samples, since s along with t are appreciably large, both exchange energy (since s is large) as well as anisotropy energy (since t is large) become very small; as a result, thermal fluctuations of core moments persist down to sufficiently low temperatures below T_C . On the contrary, for comparatively larger (average) grain size samples, since s along with t are small, exchange energy and mainly the anisotropy energy are appreciable, which causes the suppression of thermal fluctuations of core moments at relatively higher temperature than that of a smaller grain size sample. In the presence of sufficiently large scale thermal fluctuations of core moments, the conditions for SPT cannot be achieved. Therefore, under such an unfavorable condition for SPT, we observe an insulating behavior at the high-temperature ferromagnetic regime down to the temperature at which thermal fluctuations of core moments persist. Basically, it is the strong competitive interaction between magnetic exchange energy, anisotropy energy, and thermal energy that decides this blocking temperature T_B ($< T_C$). Now, at this low-temperature regime with the blocked state (or ordered) of core moments, SPT of conduction electrons takes place, creating the so-called metallic regime. So, based upon the above discussion, one may expect a steady decrease of blocking temperature T_B with a decrease in grain size, which in turn causes the observed drop in T_p as a result of decreasing grain size.

We have also carried out (ρ - T) measurements (Fig. 5) on two samples having average grain sizes of 17 and 27 nm till a lowest attainable temperature down to 20 K. At sufficiently low temperature ($\sim T=40$ K) there is a resistivity upturn (insets of Fig. 5), i.e., a minimum (T_{\min}) in ρ - T curves in the case of both the samples. This is another extrinsic effect that is not present in single crystals, but is common in polycrystalline ceramic samples. Kumar *et al.*⁵⁰ attributed this resistivity upturn, in the case of LCMO thin film, mainly to the

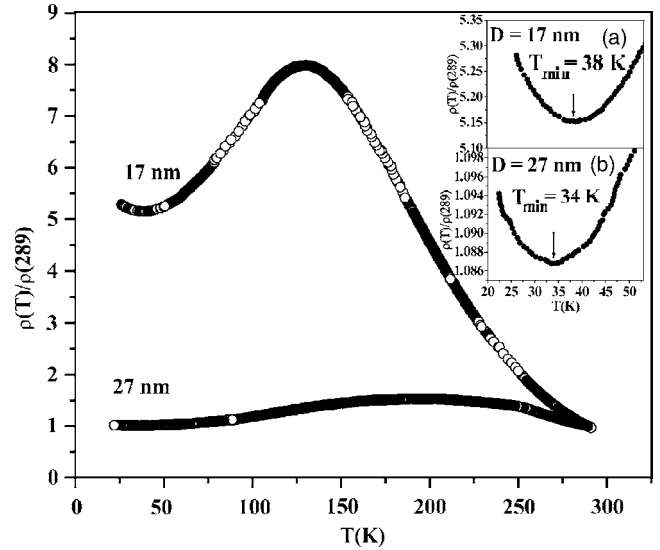


FIG. 5. Normalized reduced resistivity vs temperature for LCMO samples having average grain sizes of 17 and 27 nm down to 20 K. Insets (a) and (b) show a distinct resistivity upturn at low temperature ($T \sim 40$ K) in the normalized resistivity vs temperature curve for LCMO samples having average grain sizes of 17 and 27 nm, respectively.

electron-electron (e - e) interaction that considers the phase coherence of two electrons at low temperature, as a result of which both become localized through elastic impurity scattering. In the case of the 27 nm sample, T_{\min} occurs at 34 K whereas for the 17 nm sample it shifts to 38 K. It is noticeable that in decreasing temperature by 12 K from their respective T_{\min} , the rise in resistivity for the 17 nm sample is almost 2.5% [inset (a) of Fig. 5], whereas for 27 nm sample [inset (b) of Fig. 5] it is only 0.7%. In order to describe this sharper rise in resistivity (2.5%) for the smaller grain size sample than that of the larger grain size sample (0.7%) at low temperature, we have adopted the theoretical results as proposed by Sheng *et al.*,⁴⁸ according to which,

$$\rho(T) \approx \exp \sqrt{(\Delta/T)} \quad (1)$$

with $\Delta \sim E_C$, where E_C is the charging energy. This approach was first made by Balcells *et al.*⁴⁶ for $\text{La}_{0.7}\text{Sr}_{0.3}\text{MnO}_3$ polycrystalline samples that gave the first experimental verification of a Coulomb blockade contribution to the resistivity in granular manganese perovskites. We have fitted the $\ln \rho(T)$ versus $1/\sqrt{T}$ curve in the lowest temperature regime as shown in Fig. 6, which exhibits a linear dependence up to ~ 40 K. We obtained $E_C \sim \Delta$, from these fits as 13 K (± 0.033 K) for 17 nm sample and 0.026 K (± 0.00004 K) for 27 nm sample. So, from these fits, we may conclude that with the decrease in average grain size the contribution of Coulomb barrier [of electrostatic origin (E_C)], superimposed to the magnetic (W) and structural (e - e) one, increases which in turn cause a steeper rise in resistivity with the reduction of grain size. Thus at reasonably low temperatures (~ 40 K, in our case), the net energy barrier (E) is quite large for a sufficiently small grain size sample. As we have already mentioned, charge carriers are thermally activated; therefore, for

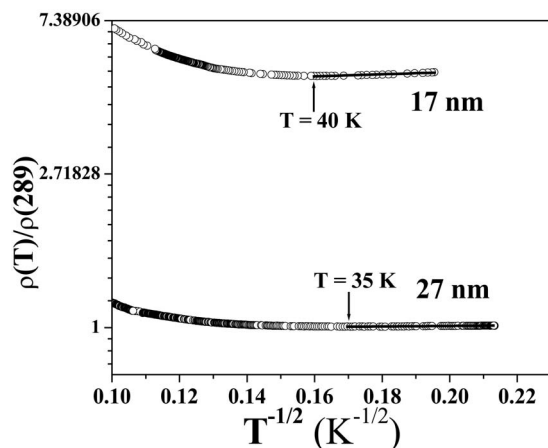


FIG. 6. Plot of $\ln \rho(T)/\rho(289)$ vs $1/\sqrt{T}$, where circles (\circ) are the experimental data points and the straight line denotes the low-temperature resistivity fit to $\rho(T) = A \exp(\sqrt{\Delta}/T)$. Slope of the fits is proportional to electrostatic Coulomb energy barrier (E_C) between nanometric grains.

nanodimensional manganites at low temperature regimes, charge carriers would have considerably lower energy (E'_C) than that of E . At very low-temperature regimes, although a favorable condition for SPT of conduction electrons which can be achieved due to the blocking or nearly ferromagnetic ordering of spins, charge carriers are inhibited from tunneling from grain to grain as they have insufficient energy ($E'_C \ll E$). Therefore, at very low temperatures, there is again a pronounced increase in resistivity, resulting in the observed upturn.

C. Magneto transport studies

Magnetoresistance (MR) measurements [Figs. 7(a) and 7(b)] show the typical magnetic field and temperature dependent behavior of MR of LCMO nanocrystals having average grain sizes of 17 and 27 nm, respectively. These curves exhibit the usual behavior of polycrystalline samples with a large low-field MR (LFMR, $H < 5$ kOe) followed by a slower varying MR at comparatively high-field regime (HFMR, $H > 5$ kOe), where MR is almost linear with H . It can be observed that at $T = 80$ K, LFMR (at $H = 3$ kOe) is about 15% for the 17 nm sample and 13% for the 27 nm sample. Figures 8(a) and 8(b) show the temperature dependence of MR, for those two samples, at $H = 3$ kOe (LFMR) and at 10 kOe (HFMR), respectively. In this nanodimensional LCMO system, we observed unprecedentedly that the magnitude of LFMR as well as of HFMR remains constant up to a sufficiently high temperature and then drops sharply with temperature. The effect gets more pronounced with the decrease in particle size, which can be clearly seen from Fig. 8. We have observed the same temperature dependent feature of MR for LSMO nanocrystalline samples,²⁵ prepared through the same preparation method. In order to explore the basic physics behind this temperature dependence of MR in our nanocrystalline LCMO sample, our primary approach is to separate out the part of the MR originating from SPT (MR_{SPT}), from the part of the MR identified by the suppres-

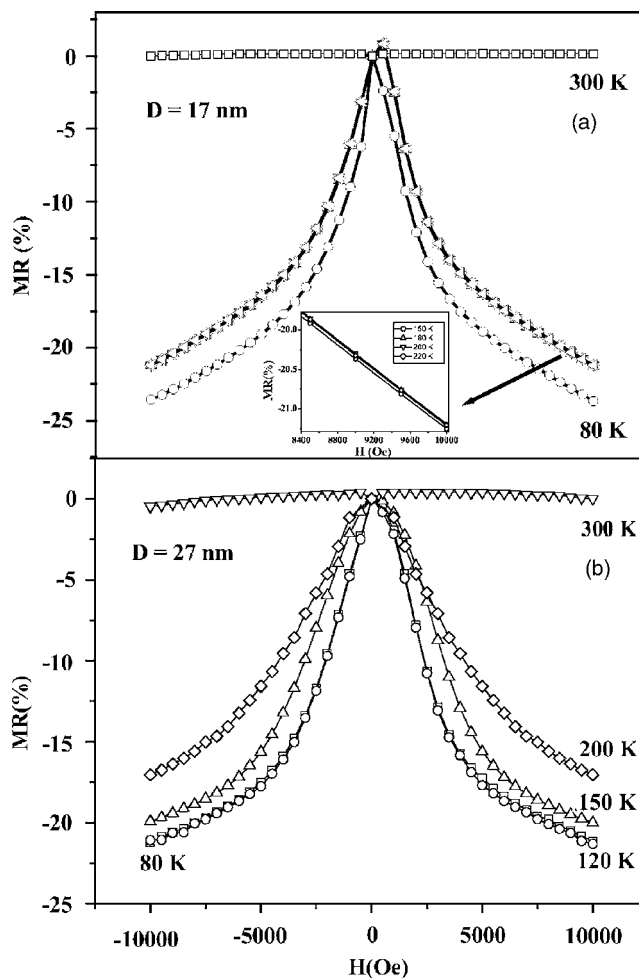


FIG. 7. Magnetoresistance as a function of magnetic field (-10 kOe, 0 , $+10$ kOe) at various temperatures (80 – 300 K) for LCMO samples having an average grain size of (a) 17 nm and (b) 27 nm.

sion of spin fluctuation (MR_{INT}) and mainly to inspect their respective temperature dependencies. For this purpose, we have used the model as proposed by Raychaudhuri *et al.*,¹² based on SPT transport of conduction electrons at the grain boundaries with attention paid to the magnetic domain wall motion at grain boundaries under the application of a magnetic field. Extending the idea of SPT as proposed by Helman and Abeles,³⁹ this model describes the magnetic field dependence of MR taking into account the gradual slippage of domain walls across the grain boundaries' pinning centers in an applied magnetic field. According to this model we get the expression for MR as

$$MR = -A' \int_0^H f(k) dk - JH - KH^3. \quad (2)$$

Within the approximation of the model, in zero field the domain boundaries are pinned at the grain boundary pinning centers having pinning strengths k . The grain boundaries have a distribution of pinning strengths (defined as the minimum field needed to overcome a particular pinning barrier) given by $f(k)$, expressed as

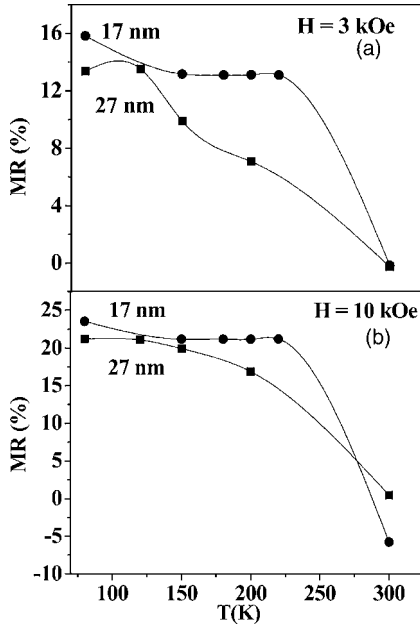


FIG. 8. Magnetoresistance as a function of temperature, ranging between 80 and 300 K, for LCMO samples having average grain sizes of 17 and 27 nm, at (a) 3 kOe and (b) 10 kOe.

$$f(k) = A \exp(-Bk^2) + Ck^2 \exp(-Dk^2). \quad (3)$$

All the adjustable fitting parameters, A , B , C , D , J , K with A' absorbed in A and C , are required to know from a nonlinear least square fitting to calculate MR_{SPT} , which is defined as

$$MR_{SPT} = - \int_0^H f(k) dk. \quad (4)$$

To fit Eq. (2) to the MR curves for those two samples having different particle sizes, we have followed the same scheme as used by Raychaudhuri *et al.*¹² Differentiating Eq. (2) with respect to H and putting Eq. (3), we get

$$\frac{d(MR)}{dH} = A \exp(-BH^2) + CH^2 \exp(-DH^2) - J - 3kH^2. \quad (5)$$

The experimental (MR- H) curves were differentiated and fitted to Eq. (5) to find the best-fit parameters at several temperatures. Figure 9(a) shows the differentiated curve and the best-fit function at $T=80$ K for LCMO sample having a grain size of 17 nm. Using the best-fit parameters we have fitted Eq. (2) [inset of Fig. 9(a)] to our experimental MR versus H curves at several temperatures. Figure 9(b) shows excellent fit for the experimental curves to Eq. (2) for samples having a particle size of 27 nm at several temperatures below T_C .

We have listed the value of experimental MR, $MR_{SPT}(H)$ [calculated using Eq. (4)] and $MR_{INT}(H)$ at $H=10$ kOe along with values of the normalized χ^2 in Table II, for nanocrystalline LCMO samples having average grain sizes of 17 and 27 nm, respectively. The χ^2 values from the fit compare favorably with experimental resolution. Figure 10 shows the temperature variation of the total experimental MR, $MR_{SPT}(H)$ and $MR_{INT}(H)$. It is evident from Fig. 10 that the magnitude of the calculated MR due to SPT, i.e., $MR_{SPT}(H)$

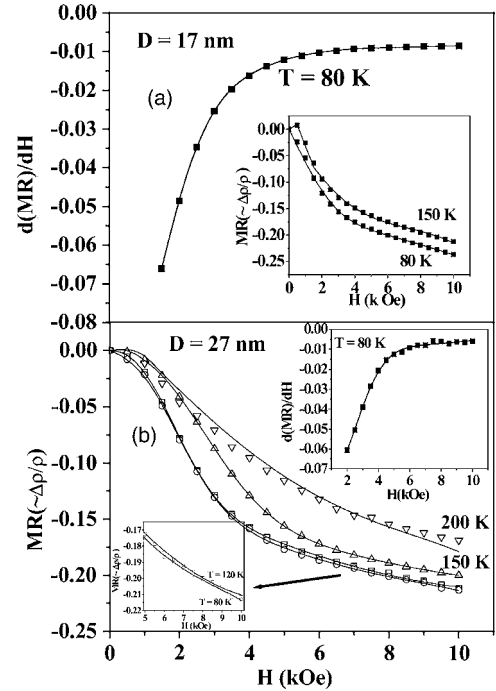


FIG. 9. (a) Derivative of the experimental (MR- H) curve (dot) and the fitted curve (line) using Eq. (5), at 80 K in the magnetic field range of (1 kOe–10 kOe) for an LCMO sample having a grain size of 17 nm. Inset shows experimental MR- H curves (dot) and the fitted curves (line) using Eq. (2), at 80 K and 150 K in the magnetic field range of (0 kOe–10 kOe) of the same sample. (b) Experimental MR- H curves (dots) and the fitted curves (lines) using Eq. (2), at various temperatures in the magnetic field range of (0 kOe–10 kOe) for the LCMO sample having an average grain size of 27 nm. Upper inset shows derivative of the experimental (MR- H) curve (dot) and the fitted curve (line) using Eq. (5), at 80 K in the magnetic field range of (1 kOe–10 kOe) of the same sample.

remains constant up to a high temperature and then drops sharply with temperature. This effect gets enhanced with the decrease in particle size. For the smallest grain size sample of 17 nm, this flat plateau region in MR versus T curves even extends up to $T \sim 220$ K. This immediately indicates the enhanced grain surface effect, which is expected to be continue increasing with decreasing particle size, as responsible for this strange temperature dependence of MR. The moment surface effect comes into picture, one can readily realize the fact that it is not the direct SPT of conduction electrons between two neighboring grains that can explain this strange phenomena. Again, the direct tunneling model, as proposed earlier by Helman and Abeles³⁹ in granular nickel films, essentially predicts a decrease of MR with increasing temperature. Thus, in order to elucidate the basic physics behind this unusual temperature dependence of MR, the dominating key factor needs to be given importance is the intermediate state of tunneling involving the grain boundary interface, which makes it sensitive to the magnetization of the surface (M_S).⁴¹ Grain surface magnetization or shell magnetization (M_S), which we assumed to be zero in the absence of any magnetic field, becomes appreciable in the presence of a magnetic field. The presence of a magnetic field will reduce the antiferromagnetism⁴⁷ at the grain surface; at considerably

TABLE II. Experimental MR, $MR_{SPT}(H)$ [calculated using Eq. (4)], $MR_{INT}(H)$ and normalized χ^2 at $H=10$ kOe at several temperatures, for nanocrystalline LCMO samples having average grain size 17 and 27 nm, respectively.

Grain size (nm)	T (K)	Expt. MR (%)	MR_{SPT} (%)	MR_{INT} (%)	χ^2
17	80	23.54	21.51	2.03	5.76×10^{-9}
	150	21.18	19.31	1.87	13.8×10^{-9}
	180	21.19	20.02	1.17	12.6×10^{-9}
	200	21.18	19.54	1.64	6.14×10^{-9}
	220	21.20	19.33	1.87	2.42×10^{-9}
27	80	21.22	20.11	1.11	6.95×10^{-7}
	120	21.09	19.59	1.50	19.5×10^{-7}
	150	19.92	16.28	3.64	0.29×10^{-7}
	200	16.88	12.28	4.60	80.9×10^{-7}

$$^a\chi^2 = \left(\frac{1}{N} \right) \sum_n^{i=1} \left[\frac{(\rho_{raw}^i - \rho_{fit}^i)^2}{(\rho_{fit}^i)^2} \right].$$

high fields, the surface spins will tend to align parallel to the bulk. To have a clear understanding about the relevancy of M_S in this case of nanodimensional manganites, we should take into consideration the nanometric grain size of our LCMO samples for which the surface-to-volume ratios of each individual grain are sufficiently large. Therefore, surface related physical properties are supposed to be very much more pronounced than its bulk counterpart. Following this, we may judiciously assert that the relevant magnetization controlling the spin-polarized tunneling is that of the surface and not the bulk. It has been reported earlier that in the nanosize regime, with the increase in surface-to-volume ratio, net magnetic behavior is dominated by surface magnetic properties.^{22–24} However, the microscopic nature of the grain surface region is not well understood so far. Moreover, there is inconsistency between several reports on the behavior of M_S of manganites grains. For example, according to Park *et al.*⁵¹ M_S is suppressed compared to the bulk magnetization, whereas Soh *et al.*⁵² reported that the T_C near the grain boundary gets enhanced, up to 20 K higher than the grain interior.

Here, however, in order to address this phenomenon, we have adopted the theoretical perspective as was reported by Lee *et al.*⁴¹ According to them, the expression for conductivity (σ) in polycrystalline perovskite manganites in the presence of a magnetic field H is given by

$$\frac{\sigma}{\sigma_0} \propto 1 + 2\vec{M} \cdot \langle \hat{S}_b \rangle + \langle (\vec{M} \cdot \hat{S}_b)^2 \rangle, \quad (6)$$

where σ_0 is the zero-field conductivity, S_b is the spin orientation at the grain boundary, and M is the normalized magnetization of the bulk spin. At high fields, Eq. (6) reduces to

$$\frac{\sigma}{\sigma_0} \approx 1 + \frac{1}{3}M^2 + 2\chi_b HM. \quad (7)$$

Here the third term yields $M^2/3$, since the third term can be written as $M^2\langle \cos^2 \theta \rangle$, where θ is the angle between S_b and

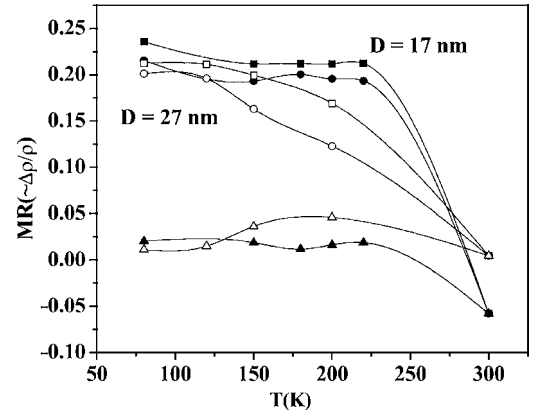


FIG. 10. Temperature dependence of the total MR (\square), calculated MR due to spin-polarized tunneling MR_{SPT} (\circ), and intrinsic contribution MR_{INT} (\triangle) at 10 kOe, for LCMO samples having average grain sizes of 17 nm (filled symbols) and 27 nm (open symbols), respectively.

M . The thermal average of the boundary spin is proportional to $\chi_b H$, where χ_b is the spin susceptibility of the boundary spins. Hence to analyze our data using this model, we have presented in Figs. 11(a) and 11(b) a detailed study of magnetoconductivity (MC), calculated as $MC = \sigma(H)/\sigma_0$, as a function of temperature and magnetic field for the 27 and 17 nm samples, respectively. Considering the model, the slope (S) of the MC versus H curve at high-field regime ($H > 5$ kOe) can be taken to be the measure of the surface spin susceptibility χ_b . Figures 11(c) and 11(d) show the high field ($H=10$ kOe) MC slope (S), i.e., χ_b , as a function of temperature for the 27 and 17 nm samples, respectively. Very interestingly, we found that S , i.e., χ_b , follows the exact nature of the temperature dependence of MR of the respective samples. This theoretical analysis indirectly supports our un-

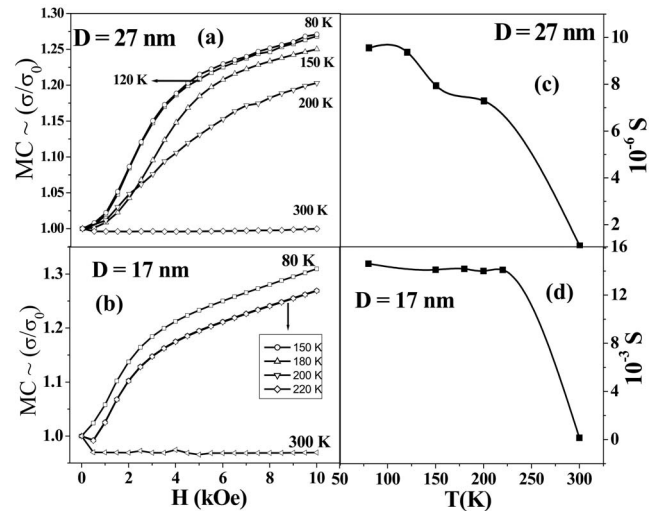


FIG. 11. Normalized conductivity as a function of magnetic field (0–10 kOe) at several temperatures (80–300 K) for LCMO samples having average grain sizes of (a) 27 nm and (b) 17 nm. (c) and (d) show the high-field MC slope (S) at 10 kOe, as a function of temperature for LCMO samples having average grain size 27 and 17 nm, respectively. The solid lines are a guide for the eye.

derstanding of the role of the M_S , which we believe to be the key factor for this unusual temperature dependent behavior of MR in our nanodimensional manganite system.

In order to give a plausible physical explanation of this temperature insensitive behavior of MR, as well as of χ_b up to considerably high temperatures, we would like to recall the fact that in the case of polycrystalline materials, grain boundaries provide defect sites where the anisotropy energy of the surface spin is minimum. So one may expect a strong pinning of surface spins at the disordered surface of polycrystalline grains. In our case, due to the nanometric grain size of our manganites samples, the surface-to-volume ratio of each individual grain is sufficiently large and, as a result, the following physical effects are most likely to take place in a higher degree. Those are: (a) contamination of the grain surface, (b) breaking of Mn-O-Mn paths at the grain surface, (c) deviation of stoichiometric composition at the grain surface, (d) termination of the crystal structure at the grain surface, and (e) dislocation at the grain boundaries. These all collectively make the surface of our nanocrystalline manganite grains full of defect sites having strong pinning strength (k) of spin at the grain surface. Figure 2(d) shows the HR-TEM image of the disordered grain surface of LCMO nanocrystals, indicating faceted grain surface. Arrows (\uparrow) in Fig. 2(d) indicate defect points at the grain surface and the (\perp) symbol represents the dislocation points at the grain boundary interface of nanosize (17 nm) LCMO grains. The existence of a distorted surface of the nanosize manganite grains has been indirectly supported by the observation of a surface phonon,⁵³ which was seen from the IR spectra for LCMO samples with small grain size. With the application of magnetic field core spins and a small fraction of surface spins, those loosely bound to the grain surface are readily aligned along the direction of magnetic field. However, as the majority of surface spins lie at the grain boundary pinning center having large pinning strength (k), final orientation of those surface spins, under the application of magnetic field, takes place as a result of a competitive interaction between grain boundary pinning strength (k) and magnetic field. As a direct consequence of this competition between these two strong forces (magnetic force and pinning force of the defect site at the grain boundary), one may think of the surface spins in a highly strained condition resulting in a blocked state at the grain surface. Thermal energy ($k_B T$), up to a considerably high temperature, is not strong enough to flip the spins from this strained condition at the grain surface. Thus, in presence of an appreciably large magnetic field, surface spin arrangements on the grain surface remain almost unaffected with the rise in temperature, which means a negligible spin-flip scattering due to thermally excited magnons. This in turn allows SPT transport to occur steadily up to a considerably high temperature, resulting in the flat plateau region in MR- T curves [Figs. 8]. Moreover, Figs. 11(c) and 11(d) show that the magnitude of S for the 27 nm sample is 10^{-3} order smaller than that of 17 nm sample. This corroborates our

above conception about the enhanced importance of M_S with reduced dimensionality of the grains. Thus, quite expectedly, we found from the experimental results [Fig. 8] that for the 17 nm sample, the flat plateau region in MR- T curves extends throughout its ferromagnetic regime ($T_C=225$ K) whereas for the 27 nm sample it starts falling beyond 150 K, i.e., at $0.6 T_C$ ($T_C=234$ K). However, a spin-polarized photoemission study, to elucidate the temperature dependence of M_S in our nanosized manganite systems, is needed for better understanding of the behavior of the surface spins of these nanometric grains.

IV. CONCLUSIONS

In conclusion, we have presented detailed studies of electrical and magnetotransport behavior of LCMO samples having a grain size of few tens of nanometer. It is found that in explaining the observed variation of T_P in case of our series of samples, we can as a whole attribute this mainly to the varying nanometric grain size, neglecting the porosity effect, whereas the observed variation in absolute value of resistivity has to be considered as due to the coupled effect of both porosity and nanometric grain size. Further, based upon SPT mechanism, we have proposed a phenomenological model to explain the gradual drop of T_P with a decrease in grain size, while T_C remains almost constant. We have attributed the steeper low-temperature (~ 40 K) resistivity upturn in the smaller grain size sample than that of larger grain size sample below their respective resistivity minima to the increased value of charging energy (E_C). Most interestingly, MR measurements show that LFMR as well as HFMR remains constant up to a sufficiently high temperature (~ 220 K) and then drops sharply with temperature. This effect gets enhanced with the decrease in particle size. We have analyzed our experimental MR data following a phenomenological model to separate out the MR arising from spin-polarized transport (MR_{SPT}), from the intrinsic contribution in our nanosize granular LCMO samples. We have observed that the magnitude of MR_{SPT} remains constant up to a sufficiently high temperature and then drops rapidly with temperature. For our smallest grain sample of 17 nm, a considerable low-field MR (15%) exists even at 220 K temperature. This is an appreciable improvement over previous work. This strange temperature dependence of MR is observed to be decided predominantly by the nature of the temperature response of surface magnetization (M_S). The strong freezing of Mn spins into a distorted state, due to random exchange interactions or random anisotropies at the surface, causes such a remarkable temperature dependent behavior of MR in these granular nanometric manganites. Though our temperature dependent MR results are far from optimal, they seem to suggest that nanosize modulation of manganite grains may lead to technologically important advances through the tuning of temperature dependent behavior of LFMR.

- *Corresponding author. Electronic address: tnath@phy.iitkgp.ernet.in
- ¹J. G. Bednorz and K. A. Müller, *Z. Phys. B: Condens. Matter* **64**, 189 (1986).
 - ²R. von Helmolt, J. Wecker, B. Holzapfel, L. Schultz, and K. Samwer, *Phys. Rev. Lett.* **71**, 2331 (1993).
 - ³T. Okuda, A. Asamitsu, Y. Tomioka, T. Kimura, Y. Taguchi, and Y. Tokura, *Phys. Rev. Lett.* **81**, 3203 (1998).
 - ⁴J.-S. Zhou, J. B. Goodenough, A. Asamitsu, and Y. Tokura, *Phys. Rev. Lett.* **79**, 3234 (1997).
 - ⁵R. A. Rao, D. Lavric, T. K. Nath, C. B. Eom, L. Wu, and F. Tsui, *Appl. Phys. Lett.* **73**, 3294 (1998).
 - ⁶Y. Suzuki, H. Y. Hwang, S. W. Cheong, and R. B. vanDover, *Appl. Phys. Lett.* **71**, 140 (1997).
 - ⁷C. W. Kwon, M. C. Robson, K.-C. Kim, J. Y. Gu, S. E. Lofland, S. M. Bhagat, Z. Trajanovic, M. Rajeswari, T. Venkatesan, A. R. Kratz, R. D. Gomez, and R. Ramesh, *J. Magn. Magn. Mater.* **172**, 229 (1997).
 - ⁸R. Mahendiran, S. K. Tiwary, A. K. Raychaudhuri, T. V. Ramakrishnan, R. Mahesh, N. Rangavittal, and C. N. R. Rao, *Phys. Rev. B* **53**, 3348 (1996).
 - ⁹H. Y. Hwang, S.-W. Cheong, P. G. Radaelli, M. Marezio, and B. Batlogg, *Phys. Rev. Lett.* **75**, 914 (1995).
 - ¹⁰*Colossal Magnetoresistive Oxides*, edited by Y. Tokura (Gordon and Breach, New York, 2000).
 - ¹¹H. Y. Hwang, S.-W. Cheong, N. P. Ong, and B. Batlogg, *Phys. Rev. Lett.* **77**, 2041 (1996).
 - ¹²P. Raychaudhuri, K. Sheshadri, P. Taneja, S. Bandyopadhyay, P. Ayyub, A. K. Nigam, and R. Pinto, *Phys. Rev. B* **59**, 13919 (1999); P. Raychaudhuri, T. K. Nath, A. K. Nigam, and R. Pinto, *J. Appl. Phys.* **84**, 2048 (1998).
 - ¹³J. Rivas, L. E. Hueso, A. Fondado, F. Rivadulla, and M. A. López-Quintela, *J. Magn. Magn. Mater.* **221**, 57 (2000).
 - ¹⁴D. G. Lamas, A. Caneiro, D. Niebieskikwiat, R. D. Sánchez, D. García, and B. Alascio, *J. Magn. Magn. Mater.* **241**, 207 (2002).
 - ¹⁵N. Zhang, W. Ding, W. Zhong, D. Xing, and Y. Du, *Phys. Rev. B* **56**, 8138 (1997).
 - ¹⁶W. C. Johnson and J. W. Cahn, *Acta Metall.* **32**, 1925 (1984).
 - ¹⁷C. L. Wang and S. R. P. Smith, *J. Phys.: Condens. Matter* **7**, 7163 (1995).
 - ¹⁸V. Biju and M. Abdul Khadar, *Mater. Sci. Eng., A* **304-306**, 814 (2001).
 - ¹⁹M. Abdul Khadar and B. Thomas, *Nanostruct. Mater.* **10**, 593 (1998), M. Abdul Khadar, *Physics of Semiconductor Nanostructures* (Narosa Publishing House, New Delhi, 1998).
 - ²⁰R. Brringer, *Mater. Sci. Eng., A* **117**, 33 (1989); H. Gleiter, *Adv. Mater. (Weinheim, Ger.)* **4**, 474 (1992).
 - ²¹A. E. Berkowitz, R. H. Kodama, Salah A. Makhoul, F. T. Parker, F. E. Spada, E. J. McNiff, Jr., and S. Foner, *J. Magn. Magn. Mater.* **196-197**, 591 (1999).
 - ²²D. L. Mills, *Phys. Rev. B* **3**, 3887 (1971).
 - ²³G. Bergmann, *Phys. Rev. Lett.* **41**, 264 (1974).
 - ²⁴J. M. D. Coey, *Phys. Rev. Lett.* **27**, 1140 (1971).
 - ²⁵P. Dey, T. K. Nath, Uday Kumar, and P. K. Mukhopadhyay, *J. Appl. Phys.* **98**, 014306 (2005).
 - ²⁶M. M. Savosta, V. N. Krivoruchko, I. A. Daniilenko, V. Yu. Tarenkov, T. E. Konstantinova, A. V. Borodin, and V. N. Varyukhin, *Phys. Rev. B* **69**, 024413 (2004).
 - ²⁷L. Balcells, B. Martínez, F. Sandiumenge, and J. Fontcuberta, *J. Magn. Magn. Mater.* **211**, 193 (2000).
 - ²⁸T. Zhu, B. G. Shen, J. R. Sun, H. W. Zhao, and W. S. Zhan, *Appl. Phys. Lett.* **78**, 3863 (2001).
 - ²⁹Y. W. Duan, X. L. Kou, and J. G. Li, *Physica B* **355**, 250 (2005).
 - ³⁰Tianhao Ji, Jiye Fang, Volodymyr Golob, Jinke Tang, and Charles J. O'Connor, *J. Appl. Phys.* **92**, 6833 (2002).
 - ³¹D. Niebieskikwiat, R. D. Sánchez, D. G. Lamas, A. Caneiro, L. E. Hueso, and J. Rivas, *J. Appl. Phys.* **93**, 6305 (2003).
 - ³²Anulekha Dutta, N. Gayathri, and R. Ranganathan, *Phys. Rev. B* **68**, 054432 (2003).
 - ³³R. Mahesh, R. Mahendiran, A. K. Raychaudhuri, and C. N. R. Rao, *Appl. Phys. Lett.* **68**, 2291 (1996).
 - ³⁴R. D. Sánchez, J. Rivas, C. Vázquez-Vázquez, A. López-Quintela, M. T. Causa, M. Tovar, and S. Oseroff, *Appl. Phys. Lett.* **68**, 134 (1996).
 - ³⁵L. E. Hueso, F. Rivadulla, R. D. Sánchez, D. Caeiro, C. Jardón, C. Vázquez-Vázquez, J. Rivas, and M. A. López-Quintela, *J. Magn. Magn. Mater.* **189**, 321 (1998).
 - ³⁶A. Urushibara, Y. Moritomo, T. Arima, A. Asamitsu, G. Kido, and Y. Tokura, *Phys. Rev. B* **51**, 14103 (1995).
 - ³⁷A. de Andrés, M. Garcia-Hernández, and J. L. Martínez, *Phys. Rev. B* **60**, 7328 (1999).
 - ³⁸S. L. Yuan, J. Tang, L. Liu, W. Chen, L. F. Zhao, Y. Tian, H. Cao, G. H. Zhang, L. J. Zhang, W. Feng, S. Liu, and Z. C. Xia, *Europhys. Lett.* **63**, 433 (2003).
 - ³⁹J. S. Helman and B. Abeles, *Phys. Rev. Lett.* **37**, 1429 (1976).
 - ⁴⁰Sheng Ju, K. W. Yu, and Z. Y. Li, *Phys. Rev. B* **71**, 014416 (2005).
 - ⁴¹S. Lee, H. Y. Hwang, Boris I. Shraiman, W. D. Ratcliff II, and S.-W. Cheong, *Phys. Rev. Lett.* **82**, 4508 (1999).
 - ⁴²M. P. Klug and L. E. Alexander, *X-ray Diffraction Procedure for Polycrystalline and Amorphous Materials* (Wiley, New York, 1974), p. 634.
 - ⁴³R. D. Sánchez, J. Rivas, D. Caeiro, M. Östlund, M. Servin, C. Vázquez, M. A. López-Quintela, M. T. Causa, and S. B. Oseroff, *Mater. Sci. Forum* **831**, 235 (1997).
 - ⁴⁴C. Zener, *Phys. Rev.* **82**, 403 (1951).
 - ⁴⁵M. Viret, M. Drouet, J. Nassar, J. P. Contour, C. Fermon, and A. Fert, *Europhys. Lett.* **39**, 545 (1997).
 - ⁴⁶L. Balcells, J. Fontcuberta, B. Martínez, and X. Obradors, *Phys. Rev. B* **58**, R14697 (1998).
 - ⁴⁷M. J. Calderón, L. Brey, and F. Guinea, *Phys. Rev. B* **60**, 6698 (1999).
 - ⁴⁸Ping Sheng, B. Abeles, and Y. Arie, *Phys. Rev. Lett.* **31**, 44 (1973).
 - ⁴⁹W. Luo, S. R. Nagel, T. F. Rosenbaum, and R. E. Rosensweig, *Phys. Rev. Lett.* **67**, 2721 (1991).
 - ⁵⁰D. Kumar, J. Sankar, J. Narayan, Rajiv K. Singh, and A. K. Majumdar, *Phys. Rev. B* **65**, 094407 (2002).
 - ⁵¹J.-H. Park, E. Vescovo, H.-J. Kim, C. Kwon, R. Ramesh, and T. Venkatesan, *Phys. Rev. Lett.* **81**, 1953 (1998).
 - ⁵²Y.-A. Soh, G. Aeppli, N. D. Mathur, and M. G. Blamire, *Phys. Rev. B* **63**, 020402(R) (2000).
 - ⁵³L. Zheng, K. B. Li, and Y. H. Zhang, *Phys. Rev. B* **58**, 8613 (1998).